

Quantitative Analysis of the Incorporation Behaviors of Sr and Ti Atoms During the Atomic Layer Deposition of SrTiO₃ Thin Films

Min Jung Chung,^{†,||} Woojin Jeon,^{†,‡,||} Cheol Hyun An,[†] Sang Hyeon Kim,[†] Yoon Kyeong Lee,[†] Woongkyu Lee,^{*,†,§} and Cheol Seong Hwang^{*,†,§}

[†]Department of Materials Science and Engineering and Inter-University Semiconductor Research Center, Seoul National University, Seoul 08826, Republic of Korea

[‡]Department of Materials Science and Engineering, Dankook University, Cheonan, Chungnam 31118, Republic of Korea

[§]Department of Materials Science and Engineering, Northwestern University, Evanston, Illinois 60208, United States

S Supporting Information



ABSTRACT: The atomic layer deposition (ALD) of multication oxide films is complicated because the deposition behaviors of the component oxides are not independent of one another. In this study, the Ti and Sr atom incorporation behaviors during the ALD of SrTiO₃ films were quantitatively examined via the carefully designed ALD process sequences. H₂O and O₃ were adopted as the oxygen sources of the SrO subcycles, whereas only O₃ was used for the TiO₂ ALD subcycles. Apart from the general conjecture on the roles of the different types of oxygen sources, the oxygen source that was adopted for the subcycles of the other component oxide had almost complete control of the metal atom incorporation behaviors. This means that the first half-cycle of ALD played a dominant role in determining the metal incorporation rate, which revealed the critical role of the steric hindrance effect during the metal precursor injection for the ALD rate. O₃ had almost doubled its reactivity toward the Ti and Sr precursors compared with H₂O. Although these are the expected results from the common knowledge on ALD, the quantitative analysis of the incorporation behaviors of each metal atom provided insightful viewpoints for the ALD process of this technically important oxide material. Furthermore, the SrTiO₃ films with a bulk dielectric constant as high as 236 were obtained by the Ru–SrTiO₃–RuO₂ capacitor structure.

KEYWORDS: atomic layer deposition, SrTiO₃, process sequence, oxygen source, incorporation rate, crystallization, DRAM capacitor

1. INTRODUCTION

Atomic layer deposition (ALD) is a critically important thin-film growth method for various electronic, energy, environment, bio, and display devices because of its (sub)atomic thickness controllability, low growth temperature, and highly uniform growth on extremely three-dimensional structures.^{1–5} These properties are due to the self-limited growth nature being ascribed to the ALD-specific surface chemistry. The ALD of many functional thin oxide films is actively being studied. The earlier reports on the ALD mechanisms and applications mainly focused on the relatively simple ALD materials, such as Al₂O₃,⁶ ZnO,^{7,8} and TiO₂,^{9,10} using simple precursors (AlCl₃, ZnCl₂, and TiCl₄) and H₂O as the oxygen source. The recent advancements in synthetic chemistry and the requirements for a better functionality of the materials for the aforementioned applications render the use of multication oxide thin films grown via ALD using metal organic precursors highly necessary.

In contrast to the simple and reliable ALD reactions between the chloride-based metal precursors and H₂O for conventional oxides,^{6–10} complex behaviors observed in the ALD reactions of the recently developed oxides with advanced functionality revealed potential difficulties in understanding on their precise mechanisms and stable operations of the deposition process.

The ALD of SrTiO₃ (STO) films, which have been explored as the ultimate high-*k* dielectric films for capacitors in dynamic random access memory (DRAM), are a typical example of such a difficulty. The ALD of STO films can be achieved by alternatively depositing SrO and TiO₂ sublayers(s), whose cycle ratios can be varied depending on the adopted precursors and the detailed process conditions.^{11–19} Among the two

Received: December 10, 2017

Accepted: February 22, 2018

Published: February 22, 2018

component oxides, the ALD of SrO films has been especially challenging because of the limited availability of precursors with high volatility primarily due to the tendency of Sr complexes to form oligomeric compounds as a result of the large size and +2 oxidation state of the group 2 elements.^{11,12,15,16,18,25,26} Tetramethylheptanedionate (tmhd)-based Sr precursors,^{13,14,18} for example, have limited volatility and reactivity toward the H₂O oxygen source.¹⁸ The high reactivity of cyclopentadienyl (Cp)-based¹⁵ and modified amide-based¹² Sr precursors is notable, but an unstable growth behavior in the STO ALD was observed at an early stage of film growth when the precursors were combined with TiO₂ deposition sequences for high-*k* STO films.^{16,27} The recent development of the ALD process by using [Sr(demamp)(tmhd)]₂ and Ti(CpMe₃)(OMe)₃ as Sr and Ti precursors, where demamp and Me mean 1-(2-dimethylaminoethyl)-(methylamino)-2-methyl-2-propoxy and methyl groups, respectively, overcomes such difficulties and allows a highly controllable, moderate growth rate owing to the preferable properties of Sr precursors.¹²

Remaining challenges in incorporating SrO and TiO₂ into STO films originate from the interactions between the metal and the oxygen sources of each oxide. In general, the growth of one component oxide layer on top of the other component layer is not necessarily identical to the growth of the layer on the same layer by several mechanisms. First, multiple oxygen sources (i.e., H₂O, O₃, or O₂ plasma) can be employed for an individual component oxide depending on the reactivity of each precursor toward different oxygen sources.^{13,14,20,21} Moreover, the type of employed oxygen source for one component oxide could influence on the ALD behavior of the subsequent deposition of the other component oxide.^{22,23} Additionally, the different chemical reactivities of component metals toward the adopted oxygen sources could induce redox reactions between the previously deposited component oxide and the newly forming oxide.²⁰ Previous studies have shown that predeposited TiO₂ can be reduced by the chemically active Sr precursor and recovers its stoichiometric oxidation state during the subsequent oxygen source supply.^{15,24} Because the recovery reaction depends on the oxidation power of the oxygen source, insufficient oxidation may result in defects (oxygen vacancy) within the film. These complicated factors require an optimized process sequence for the ALD of multicomponent oxides.

In this work, the incorporation behaviors of Sr and Ti atoms from [Sr(demamp)(tmhd)]₂ and Ti(CpMe₃)(OMe)₃ precursors in the ALD of STO films were investigated. Quantitative analysis with variations in oxygen sources and subcycle sequences reveals the dependences of the film compositions and growth rate on surface chemistry and oxygen sources (O₃ or H₂O). The systematically designed analysis introduced here serves as complementary information to the results from *in situ* diagnostic studies such as the quartz crystal microbalance,^{28–30} quadrupole mass spectrometry,^{28,31,32} Fourier transform infrared spectroscopy,^{33,34} and X-ray photoelectron spectroscopy (XPS).^{35,36} The current work compares the final film composition and layer density estimated using a quantitative spectroscopic technique [X-ray fluorescence spectroscopy (XRF)] to study the intermolecular reaction between the precursors and the film surface under given ALD sequences composed of different ratios of SrO and TiO₂ subcycles. A simple mathematical formula to describe the incorporation rates of Sr and Ti atoms per ALD step provides a potentially useful analytical tool to interpret the growth behavior of other multicomponent ALD process. Additionally, the chemical

status of the grown films under the different conditions was carefully examined using XPS, which is compared with the crystallization behavior examined by X-ray diffraction (XRD) and transmission electron microscopy (TEM). Finally, these chemical and structural analyses were related to the electrical performance of the films. A maximum bulk dielectric constant of 236 was achieved under the optimal deposition process, with a repeated sequence of Ti precursor–O₃–Ti precursor–O₃–Sr precursor–H₂O–Sr precursor–H₂O, which was the highest value among the reported STO ALD films.

2. EXPERIMENTAL PROCEDURE

STO thin films were deposited in a traveling wave-type ALD reactor (CN1 Co., Plus-100) for a 4 in. diameter single wafer. [Sr(demamp)(tmhd)]₂ (synthesized by the Korea Research Institute of Chemical Technology) and Ti(CpMe₃)(OMe)₃ (synthesized by Air Liquide) were employed as the Sr and Ti precursors, respectively. The canisters of the [Sr(demamp)(tmhd)]₂ and Ti(CpMe₃)(OMe)₃ were heated to 50 and 80 °C, respectively, to acquire the appropriate vapor pressures of the precursors. From the previously gained knowledge about the optimal oxygen sources, O₃ was adopted for the ALD of the TiO₂ layers.^{15,37} Both H₂O and O₃ were tested for the ALD of SrO and TiO₂ layers, and it was concluded that H₂O and O₃ were appropriate for the former and latter layers because of the following reasons. Adopting O₃ for the SrO growth induced a carbon contamination problem, and the Ti precursor showed limited reactivity toward H₂O under the given ALD conditions.¹² H₂O was cooled down to 5 °C to achieve the appropriate vapor pressure, and the concentration of O₃ was kept at 250 g/m³. The SrO ALD sequence consisted of precursor injection (5 s), Ar purge (5 s), H₂O or O₃ injection (2 s), and Ar purge (5 s). The sequence for the TiO₂ ALD, on the other hand, consisted of precursor injection (3 s), Ar purge (5 s), O₃ injection (2 s), and Ar purge (5 s). These sequences were proven to be consistent with the conditions for the desired ALD-specific saturated growth of each component oxide. The saturation behaviors of SrO and TiO₂ using O₃ as an oxygen source have been evaluated in previous studies.^{12,15} A similar self-limiting growth behavior for an SrO film using H₂O as the oxygen source is described in the Supporting Information. For all experiments, the thin-film growth temperature (*T_g*) was set at 370 °C for *in situ* crystallization with the aid of a crystalline seed layer.^{11,12,25} The ALD supercycle for the STO deposition consisted of the ALD subcycles of SrO and TiO₂, with different cycle ratios to clarify the deposition behavior. The wafer with the Ru (30 nm)/Ta₂O₅ (10 nm)/Si stack was used as the substrate. The layer densities of the Sr and Ti atoms in the grown films were confirmed via XRF (Thermo Scientific, ARL QUANT'X). The physical thickness of the STO films was measured with an ellipsometer (Gaertner Scientific Corporation, L116D), where the measured thickness was calibrated through cross-sectional TEM (Tecnai Osiris, FEI) and spectroscopic ellipsometry (J. A. Woollam, ESM-300). The chemical binding states of the films were determined via XPS (Thermo VG, Sigma Probe). XRD (PANalytical, X'Pert PRO) and cross-sectional TEM were used to reveal the crystallographic structure of the deposited films. To measure the electrical properties, the metal–insulator–metal (MIM) capacitor was fabricated with a 5 nm thick RuO₂ top electrode (TE) using a metal shadow mask (with a 300 μm hole diameter). The RuO₂ TE layer was deposited by dc reactive sputtering using an Ru metal target under an Ar/O₂ gas atmosphere. On the RuO₂ TE, additional 50 nm thick Pt was deposited to improve the contact during the probing. The capacitance–voltage (*C–V*) and the leakage current density–voltage (*J–V*) curves were measured using Hewlett Packard 4140D and 4194A, respectively, at room temperature. The ac excitation frequency for the *C–V* measurement was 10 kHz. The estimated dielectric loss factor was generally <~2%. During the electrical tests, the TE was biased and the bottom electrode was grounded.

Table 1. Layer Density of Ti and Sr Cations in Deposited SrTiO₃ Films with Various Sequences^a

no.	sequence	layer density of total film ($\mu\text{g}/\text{cm}^3$)	incorporation rate of Ti ($\mu\text{g}/\text{cm}^2$ per cycle)			incorporation rate of Sr ($\mu\text{g}/\text{cm}^2$ per cycle)			Sr/[Sr + Ti] (%)	remark
			layer density of Ti ($\mu\text{g}/\text{cm}^2$)	R_T^{OTO}	R_T^{HTO}	layer density of Sr ($\mu\text{g}/\text{cm}^2$)	R_S^{OSO}	R_S^{OSH}		
1	[TO] × 40	0.84	0.84	0.021						
2	[SO] × 40	2.16			2.16	0.050				
3	[SH] × 40	0.56			0.56			0.014		
4	[TOSO] × 40	2.25	0.80	0.020	1.45	0.036			50	
5	[TOTOSOSO] × 20	2.32	0.81	0.020	1.51	0.037			50	
6	[TOSH] × 40	2.04	0.56		1.48		0.037		59	
7	[TOTOSHSH] × 20	1.66	0.62	0.020	1.04		0.037	0.015	48	R_T^{HTO} from 8 for R_T^{OTO} , R_S^{OSH} from 8 for R_S^{HSH}
8	[TOSHS] × 42	2.61	0.47		2.14		0.037	0.014	71	R_S^{OSH} from 6 for R_S^{HSH}
9	[TOTOTOSH] × 13	1.25	0.73	0.019	0.52		0.038		28	10 for R_T^{OTO} and R_T^{HTO}
10	[TOTOTOTOTOSH] × 7	1.02	0.76	0.018	0.26		0.038		16	9 for R_T^{OTO} and R_T^{HTO}
11	[TOTOTOSHS] × 14	1.52	0.72	0.020	0.80		0.038	0.020	38	12 for R_T^{OTO} and R_T^{HTO} , R_S^{OSH} from 9 for R_S^{HSH}
12	[TOTOTOTOTOSHS] × 7	1.17	0.77	0.019	0.40		0.038	0.020	22	11 for R_T^{OTO} and R_T^{HTO} , R_S^{OSH} from 10 for R_S^{HSH}
13	[TOTOTOSO] × 14	1.3	0.79	0.019	0.51	0.037			26	

^a R_T^{OTO} and R_S^{OSO} mean the overall Ti and Sr incorporation rates, respectively, whose values are measured by XRF. The incorporation rates by each step (such as R_T^{OTO} and R_T^{HTO}) are calculated. Layer density of SrTiO₃ films deposited by various sequences and their cation ratio.

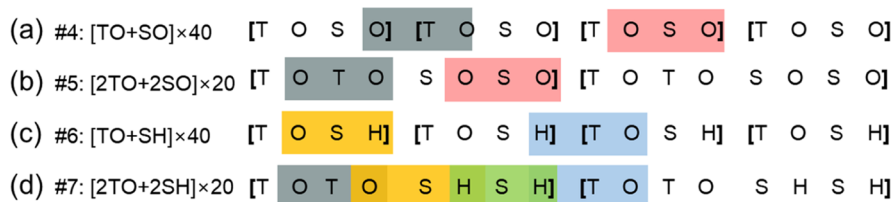


Figure 1. Schematic diagram for the precursor and oxygen source injection sequences for the sample (a) #4 [TOSO], (b) #5 [TOTOSOSO], (c) #6 [TOSH], and (d) #7 [TOTOSHSH], respectively, shown in Table 1. The brackets mean a single supercycle, and the colored backgrounds indicate the different types of oxygen sources before and after Sr or Ti precursor injection steps.

3. RESULTS AND DISCUSSION

It was previously reported that the deposited amount of Sr and Ti atoms in STO ALD could be affected by the oxygen source of SrO ALD.^{16,37,38} To first confirm this behavior, four samples were prepared, wherein the STO ALD supercycles consisted of the same number of SrO and TiO₂ ALD subcycles (20 each) with various sequences and different oxygen sources for SrO ALD, denoted as samples #4, 5, 6, and 7 in Table 1. Here, TO, SO, and SH correspond to the ALD subcycle for TiO₂ with O₃ as the oxygen source, SrO with O₃ as the oxygen source, and SrO with H₂O as the oxygen source, respectively. Although the total number of ALD cycles was identical (40), the total layer density and the Sr/[Sr + Ti] ratio, which should be 50% for obtaining desirable properties, such as high crystallinity, of STO films¹⁶ are quite different. When O₃ was used for both subcycles (samples #4 and #5), there was no notable change in the layer density and film composition, but when the SrO layer growth was performed with the SH process (samples #6 and #7), that is, H₂O was adopted for the SrO layer ALD, the total layer density decreased quite significantly (samples #4, #5 vs, #6, and #7). It was quite notable, however, that such a decrease

was due to the decrease in the growth of the TiO₂ layer (sample #6, [TOSH] × 40) and not by the decrease in the growth of the SrO layer, notwithstanding the fact that the TiO₂ ALD conditions were not varied. As a consequence, the film became Sr-rich (Sr/[Sr + Ti] ratio = 58%). When the SH step was incorporated two times (sample #7, [TOTOSHSH] × 20), the total layer density further decreased, which can now be ascribed to the large decrease in the SrO layer density, whereas the TiO₂ growth was actually slightly enhanced compared to sample #6. These results suggest that the ALD behaviors of the component layers mutually influenced each other, especially when the oxygen source varied. To more systematically examine such behaviors, the following analysis and additional experiments were performed.

Figure 1 shows the schematic diagram of the precursor and oxygen source injection sequences for the samples #4, #5, #6, and #7. The colored backgrounds indicate the different types of oxygen sources injected before and after the Sr or Ti precursor injection step. For the case of sample #4 ([TOSO] × 40), all oxygen sources are O₃; as such, the ALD sequence is actually a repetition of the OTO (gray) and OSO (red) steps. The same holds true for the process of sample #5, [TOTOSOSO] × 20.

In the case of sample #6, it is the repetition of the HTO (blue) and OSH (yellow) steps. For sample #7 ([TOTOSHS] × 20), however, four different types of steps [OTO (gray), OSH (yellow), HSH (green), and HTO (blue)] are involved. It is considered that the types of oxygen sources injected before the metal precursor injection determine the first half-cycle of ALD, whereas the oxygen source injected after the metal precursor injection completes the remaining ALD half-cycle (actually, the SrO or TiO₂ subcycle). Therefore, from this viewpoint, both types of oxygen sources could have a critical influence on the metal incorporation behavior. In addition, one ALD subcycle covers only a certain portion of the surface, so there remain plenty of heterogeneous film surface sites (i.e., the TiO₂ surface for the SrO subcycle and vice versa).² When the second ALD subcycle is performed, it could be surely assumed that the additional film growth can occur both on the remaining heterogeneous film surface as well as on the homogeneous film surface that was grown in the previous ALD subcycle step. In the case of Figure 1, there are five variables (OTO, OSO, OSH, HTO, and HSH) to be determined, but only four equations can be set up, meaning that the five variables cannot be explicitly calculated and additional experiments are needed. Nonetheless, there must be another critical point that should be taken into account to correctly interpret the incorporation behaviors. One, the ALD subcycle usually produces a submonolayer, and as such, not only the immediate previous ALD layer but also the one (or two or even more) prior to that can affect the subsequent ALD subcycle.² For example, for the case of sample #6 ([TOSH] × 40 process), when the Ti precursor was injected, the surface most likely consisted of TiO as well as SrO bondings because one SrO ALD step cannot fully cover the surface. By contrast, for the case of sample #7 ([TOTOSHS] × 20), because one more SrO subcycle existed before the Ti precursor injection of the first TO was made, the surface probably has a higher chance of having a higher portion of SrO bonding than the [TOSH] × 40 case, and as such, the incoming Ti precursor molecules behaved differently from the previous case. Therefore, the additional experiments should be carefully designed to examine all of these additional effects.

Figures 2 and 3 show the designed ALD sequences for the aforementioned purposes. The experiments shown in Figure 2

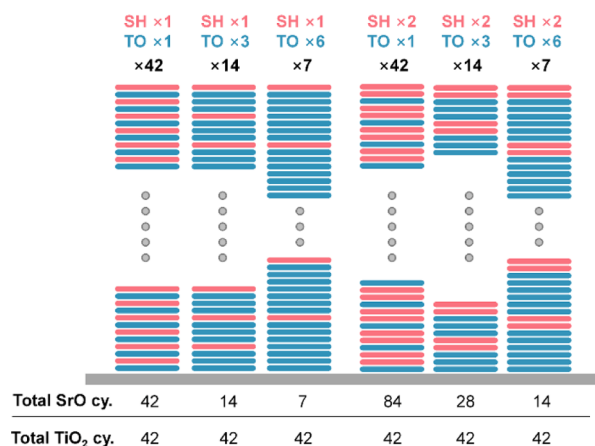


Figure 2. Schematic diagram of the designed SrTiO₃ ALD sequences to examine the influence of the SH subcycle to the Ti incorporation rate. The blue and red-colored lines indicate the TiO₂ ALD subcycle with an O₃ oxygen source (TO) and SrO ALD subcycle with an H₂O oxygen source (SH), respectively.

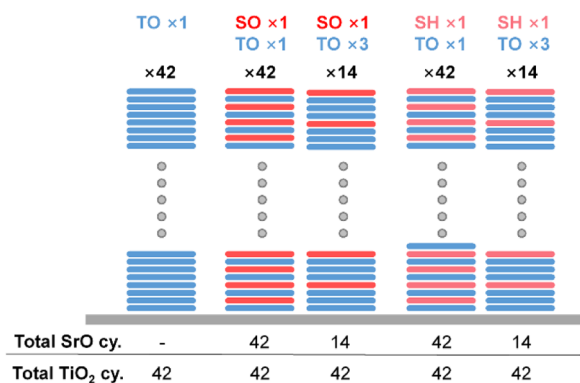


Figure 3. Schematic diagram of the designed SrTiO₃ ALD sequences to examine the influence of different types of oxygen sources (H₂O or O₃) for the SO step on the TO process. The blue and red-colored lines indicate the TiO₂ ALD subcycle with an O₃ oxygen source (TO) and SrO ALD subcycle with an O₃ oxygen source (SO), respectively.

were designed to examine the just mentioned effect; in the cases of the first three experiments, consecutive TO cycles with different numbers (1, 3, and 6) were performed on a single SH subcycle, and for the last three cases, the same TO cycles were performed on two SH subcycles. The purpose of the experiment sets shown in Figure 3 is similar to that of the experiment sets shown in Figure 2, but in this case, the influence of different types of oxygen sources (H₂O or O₃) for the SO step on the TO process can be examined.

All of the experimental results are summarized in Table 1, where the layer density values of the total film are the experimental values, and the data for OTO, HTO, OSO, OSH, and HSH are calculated as follows. For sample #9 ([TOTOTOSH] × 13), for example, the ALD subcycles for the TiO₂ growth consist of two OTO steps ([TOTOTOSH]) and one HTO step (...SH)[TOTOTOSH][TO...]. Therefore, the overall Ti incorporation rate (R_T^o) can be expressed as

$$R_T^o = (2R_T^{\text{OTO}} + R_T^{\text{HTO}}) \times 14 \quad (1)$$

where R_T^{OTO} and R_T^{HTO} are the Ti incorporation rates of the OTO and HTO steps, respectively. Similarly, the R_T^o for sample #10 ([TOTOTOTOTOSH] × 7) can be expressed as

$$R_T^o = (5R_T^{\text{OTO}} + R_T^{\text{HTO}}) \times 7 \quad (2)$$

because five OTO steps ([TOTOTOTOTOSH]) and one HTO step (...SH)[TOTOTOTOTOSH][TO...] were involved in one supercycle. For these cases, the two variables can be calculated from the two equations, and the results are reflected in the R_T^{OTO} and R_T^{HTO} columns of Table 1 for the Ti layer density part. Similar calculations can be made for several other combinations. The combinations were selected among the samples, which have a similar supercycle configuration, for the accurate calculation to exclude any effect induced by surface chemistry differences such as the nucleation incubation effect or the initial growth enhancement by the substrate (remark column in Table 1). From the calculations, the R_T^{OTO} and R_T^{HTO} were 0.018–0.020 and 0.011–0.014 $\mu\text{g cm}^{-2}$, respectively. This reveals that the incorporation rate of Ti atoms heavily depends on the type of oxygen source used in the previous ALD step, even for the given oxygen source injected after the Ti precursor injection (O₃). The higher value of R_T^{OTO} compared with R_T^{HTO} suggests that the first ALD half-reaction when the Ti precursor

was injected is more efficient on the O_3^- or O-terminated surface than on the H_2O - or OH-terminated surface, which appears reasonable, considering the higher chemical activity of O_3 compared with H_2O .^{13,14,18,20} The $R_{\text{T}}^{\text{OTO}}$ for the TiO_2 single layer (sample #1) can be straightforwardly obtained from the total Ti layer density and the number of OTO cycles, and the value was $0.021 \mu\text{g cm}^{-2}$. This is similar to the value obtained from samples #9 and #10. In fact, the $R_{\text{T}}^{\text{OTO}}$ values from all samples are quite similar ($\sim 0.020 \mu\text{g cm}^{-2}$), suggesting the robustness of this subcycle. $R_{\text{T}}^{\text{HTO}}$, however, has a different property. From Table 1, it can be understood that it has two values, 0.014 and $0.011 \mu\text{g cm}^{-2}$, whose difference is about 30% (certainly over the experimental error range) of the lower value. Looking at the supercycle constitution where the smaller value was achieved, it can be understood that the SH step was performed two times consecutively (samples #7, 8, 11, and 12), implying that the surface has higher coverage with the OH-terminated SrO layers. For the TO process step after the single SH step (samples #6, #9, and #10), the surface will be composed of O_3^- or O-terminated TiO bonds and OH-terminated SrO bonds because the single SH step could not fully cover the surface. This is in line with the finding that the first ALD half-reaction of the TiO_2 layer growth is more activated on the O_3^- or O-terminated surface than on the OH-terminated surface. The full monolayer coverage of the TiO_2 layer in STO is $\sim 0.052 \mu\text{g cm}^{-2}$ (in terms of the layer density of the Ti element), and as such, all Ti incorporation rates in Table 1 correspond to the submonolayer growth rate.

A similar analysis was performed for $R_{\text{S}}^{\text{OSO}}$, $R_{\text{S}}^{\text{OSH}}$, and $R_{\text{S}}^{\text{HSH}}$, which stand for the Sr incorporation rates for the OSO, OSH, and HSH steps, respectively. There are several significant findings from the Sr layer density parts in Table 1. First, the $R_{\text{S}}^{\text{OSO}}$ for the SO process (sample #2; $0.050 \mu\text{g cm}^{-2}$) (i.e., the SrO single layer) was the highest among all Sr incorporation rates. Second, the $R_{\text{S}}^{\text{OSO}}$ decreased to $0.036\text{--}0.037 \mu\text{g cm}^{-2}$ when the TO steps were involved (samples #4, #5, and #13), suggesting that the first ALD half-reaction on the TiO surface was less active compared with the surface with SrO bonding even for the given O_3^- or O-terminated condition. Third, the $R_{\text{S}}^{\text{OSH}}$ value was quite similar to the $R_{\text{S}}^{\text{OSO}}$ value ($0.037\text{--}0.038 \mu\text{g cm}^{-2}$). This is a very notable finding from this work; it means that the first half-reaction really governs the whole ALD process of the SrO layer. The types of oxygen sources injected after the Sr precursor pulse influence the subsequent Ti incorporation making a difference in $R_{\text{T}}^{\text{OTO}}$ and $R_{\text{T}}^{\text{HTO}}$ but does not influence the Sr incorporation itself, which is consistent with the idea that the Sr incorporation rate is mainly determined by the adsorption amount during the Sr precursor pulse step in the first ALD half-reaction. Fourth, the $R_{\text{S}}^{\text{HSH}}$ is much lower than even half of the $R_{\text{S}}^{\text{OSO}}$ and $R_{\text{S}}^{\text{OSH}}$ (samples #3, #7, #8, #11, and #12; $0.014\text{--}0.020 \mu\text{g cm}^{-2}$), suggesting the lower ALD activity of the Sr precursor toward the OH-terminated surface. Thus, the surface termination, by O_3 or H_2O , can only affect the Sr incorporation rate, resulting in that the $R_{\text{S}}^{\text{OSO}}$ and $R_{\text{S}}^{\text{OSH}}$ were not influenced by the cycle number of TO in the supercycle. The consistent values of $R_{\text{S}}^{\text{HSH}}$ for samples #3, #7, and #8 suggest that it does not matter whether it is TiOH or SrOH for the chemisorption of the Sr precursor. Nevertheless, it obviously increased to $0.020 \mu\text{g cm}^{-2}$ from $0.014 \mu\text{g cm}^{-2}$, which is certainly beyond the experimental error range, when the previous TO cycle number was over three (samples #11 and #12). As this TO subcycle number corresponds to a fully covered TiO_2 layer before the two consecutive SH steps were

performed, this fully covered TiO_2 layer will affect to the growth of the SrO layer even when H_2O was adopted for the SrO growth. The full monolayer coverage of the SrO layer in STO is $\sim 0.095 \mu\text{g cm}^{-2}$, (in terms of the layer density of the Sr element) and as such, all Sr incorporation rates in Table 1 correspond to the submonolayer growth rate. Although one monolayer of TiO_2 will not completely block the oxygen diffusion from the bottom layer to the film surface, this amount was enough to show the corresponding effect in this study because the SrO did not form a complete monolayer itself with no more than two subcycles.²

It has been reported that the high chemical reactivity between the already grown oxide layer and the metal ions in the incoming precursor can induce the enhanced growth rate of the ALD layers.^{16,38} A typical example of this was the almost chemical vapor deposition-like growth of the SrO layer during the early stage of ALD on the RuO_2 film substrate.^{16,24} As the Sr–O bonding energy is much higher than that of Ru–O, the SrO layer was fluently grown only when the Sr precursor was pulsed (before the subsequent oxygen source pulse), wherein the RuO_2 layer played the role of the oxygen source. As a consequence, the RuO_2 layer with a significant thickness was reduced to Ru only after the Sr precursor pulse. For Sr and Ti elements, as the bonding energy of Ti–O is lower than that of Sr–O (-417.0 vs -530.9 kJ/mol oxygen at 600 K), a higher portion of TiO_2 on the surface can induce higher SrO growth by donating oxygen atoms from the TiO_2 layer to the Sr precursor when the Sr precursor is injected.¹⁶ Although the HSH step was performed after the OSH step in samples #11 and #12, the single OSH step did not even fully cover the TiO_2 surface, and as such, there was certainly a high chance for a chemical reaction to occur between the underlying TiO_2 layer and the incoming Sr precursor. If this was the case, the underlying TiO_2 layer will be slightly reduced after the Sr precursor pulse step, which was indeed the case, as shown by the XPS data for the Ti 2p spectra in Figure 4.

Figure 4a–d shows the Ti 2p XPS spectra (data points) of the STO films deposited by the [TOSO] \times 40, [TOTOTOSO] \times 14, [TOTOSHSH] \times 20, and [TOTOTOSH] \times 13 sequences, respectively. From now on, [TOTOSHSH] was mainly studied instead of [TOSH] because of the substrate deterioration issue of the [TOSH] sequence, which is out of the scope of this study. Also shown in the same figures are the deconvoluted spectra (lines), assuming that the Ti 2p peaks were composed of two sets of Ti $2p_{3/2}$ and Ti $2p_{1/2}$ doublets. The mainly contributed peak was centered at the 458.5 eV binding energy (BE),³⁹ which was contributed by the stoichiometric TiO_2 . The minor peak was also exhibited from the deconvolution with a relatively lower BE of ~ 457.5 eV, suggesting that there was a contribution from the less oxidized Ti compared to TiO_2 , which was the oxygen-deficient TiO_{2-x} .³⁹ Indeed, the peak contributed by TiO_{2-x} was observed in the XPS spectra of all STO film samples, whereas TiO_{2-x} had no contribution in the Ti $2p_{3/2}$ peak of the ALD TiO_2 thin film grown using only the TO sequence (data not shown). Therefore, the existence of the TiO_{2-x} phase can be considered as the evidence of the reaction between the Sr precursor and oxygen in the TiO_2 . In the case of the [TOTOSHSH] sequence, the peak contribution by TiO_{2-x} to Ti $2p_{3/2}$ was as high as 8.8%, which was much higher than that in the [TOSO] sequence (3.9%). When the Sr precursor was pulsed after the TO step, the chemical reaction between TiO_2 and the Sr precursor will be similar, if any, irrespective of the type of

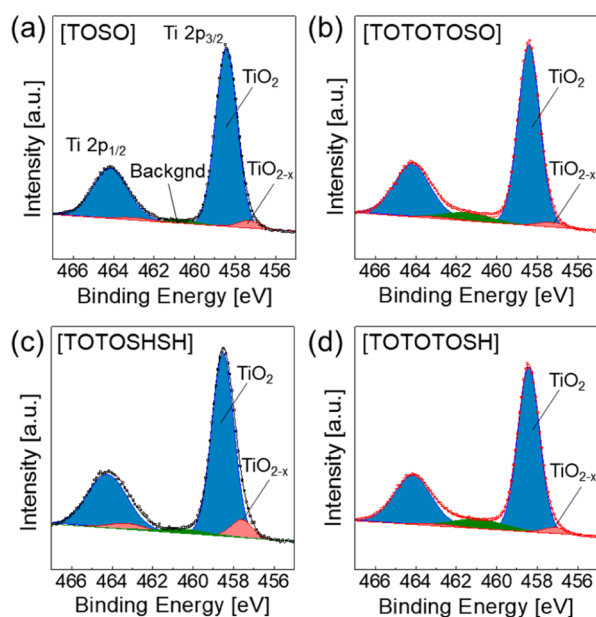


Figure 4. Peak fits of Ti 2p spectra of STO films deposited by (a) [TOSO], (b) [TOTOTOSO], (c) [TOTOSHSH], and (d) [TOTOTOSH]. The deconvoluted stoichiometric TiO_2 peak is indicated as blue color, and the oxygen-deficient phase, TiO_{2-x} , is shown in red color. The green peaks are from the background. Peak deconvolution was conducted with Ti $2p_{3/2}$ spectra (right-side peaks), and left-side peaks originated from Ti $2p_{1/2}$.

subsequent oxygen source injected. Therefore, the lower portion of TiO_{2-x} for the case of [TOSO] suggests that the TiO_{2-x} was reoxidized by the following O_3 pulse. This observation was well-corroborated by the results of the XPS spectra of the [TOTOTOSH] and [TOTOTOSO] sequences. The TiO_{2-x} ratio of the [TOTOTOSH] sequence was $\sim 3.8\%$. In this case, the single Sr pulse after three TO subcycles will induce a significant amount of TiO_{2-x} which cannot be reoxidized by the subsequent H_2O pulse step; as such, the XPS signal for TiO_{2-x} should have been higher. The TiO_2 layer during the first two TO subcycles, however, had a higher chance of maintaining the TiO_2 configuration; as such, the overall contribution from the TiO_{2-x} will be lower. In addition, the following three TO cycles have a higher possibility to reoxidize the reduced TiO_{2-x} layer than the two cycles of TO after reduction by two Sr precursor injections in the [TOTOSHSH] process. The lowest TiO_{2-x} ratio (3.1%) was achieved in the case of the [TOTOTOSO] sequence, which can be readily understood from the reoxidation effect, as for the case of the [TOSO] sequence. The TiO_{2-x} component might be contributed from both Ti^{3+} and the slightly reduced Ti^{4+} oxidation states.⁴⁰ Such a conclusion can be supported by the Sr 3d XPS spectra as shown below. More importantly, the Sr 3d XPS spectra provide critical information on the detailed crystallization behavior from the chemical point of view, which cannot be easily obtained from XRD and TEM.

The Sr 3d XPS spectra of the STO films (Figure 5) were also deconvoluted to two sets of Sr $3d_{5/2}$ and $3d_{3/2}$ doublets with an energy separation of ~ 0.9 eV and a branching ratio of 1.5. The peak centered at the 131.9 eV BE corresponds to the bulk region of the STO perovskite lattice, which is referred to as the “lattice” component, and the peak at 132.1 eV corresponds to the Sr ions in nonperovskite phases, such as SrO, $\text{Sr}(\text{OH})_2$, or SrCO_3 , which are mostly present on the film surface, so it is

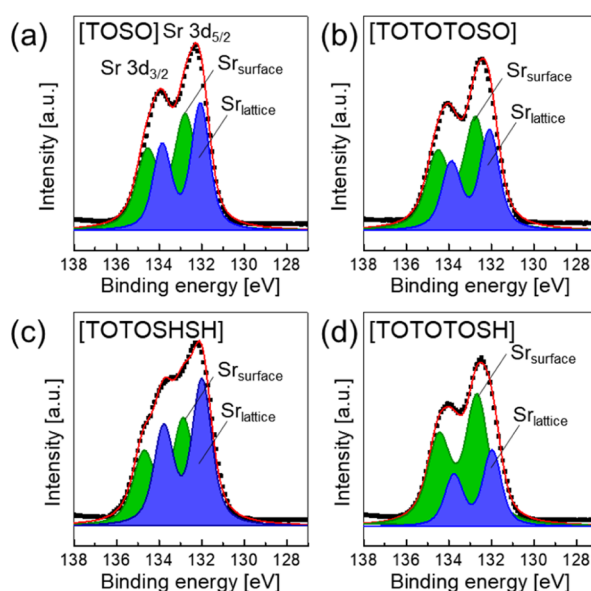


Figure 5. Peak fits of Sr 3d spectra of STO films deposited by (a) [TOSO], (b) [TOTOTOSO], (c) [TOTOSHSH], and (d) [TOTOTOSH]. The deconvoluted Sr peak from the perovskite lattice is indicated as blue color, and Sr from a surface such as SrO is shown as green color. Peak deconvolution was conducted with Sr $3d_{5/2}$ spectra (right-side peaks), and left-side peaks originated from Sr $3d_{3/2}$.

referred to as the “surface” component.^{41–43} Apart from the Ti $2p_{3/2}$ XPS spectra analysis in Figure 4, which is determined by the degree of oxidation of Ti ions, the analysis of Sr 3d XPS spectra is critically determined by the overall crystallization of the STO material, which should be largely influenced by the overall Sr/[Sr + Ti] ratio of the film. In the cases of [TOTOTOSO] and [TOTOTOSH] sequences (Figure 5b,d), the contribution by the surface component is even larger than the lattice component, which should be related to the highly nonstoichiometric composition of the deposited STO film. The calculated values of Sr/[Sr + Ti] of the STO film by [TOTOTOSO] and [TOTOTOSH] sequences are 0.26 and 0.28, respectively (Table 1), which are quite unfavorable for the crystallization of the film into the perovskite structure.¹⁶ Therefore, these samples are disregarded for further discussion on the influence of the defective layer composition on the crystallization into perovskites as shown below. For the cases of [TOSO] and [TOTOSHSH] sequences, the Sr/[Sr + Ti] ratio was 0.50 and 0.48, respectively, which are close to the desired value of 0.5.

The proportions of the Sr 3d XPS spectra from the lattice component contribution were 42.7 and 53.5% for [TOSO] and [TOTOSHSH], respectively (Figure 5a,c). It is interesting to note that the [TOTOSHSH] sample has a higher contribution from the perovskite phase despite its Sr/[Sr + Ti] value of 0.48 compared with the TOSO sample (0.50). It is further notable that the [TOTOSHSH] showed the highest TiO_{2-x} contribution in Figure 4 (8.8%). As discussed in Figure 4, the adsorbed Sr precursor can react with the previously grown TiO_2 layer, resulting in the formation of TiO_{2-x} which can be reoxidized during subsequent oxygen source feeding steps. However, in the [TOTOSHSH] sequence, the abundant amount of TiO_{2-x} remained in the STO film, indicating that the Ti atoms remained at a more chemically unstable state during the deposition of the SrO subcycle. For the case of ALD of the STO film, the perovskite phase formation should be proceeded

by the chemical reaction between the component oxide layers of TiO₂ and SrO with the aid of the thermal energy obtained by the high temperature during the ALD process. Because the film was in situ crystallized by the relatively high growth temperature (370 °C) with the help of crystalline seed layers,^{11,12,25} the active chemical interaction between the two component layers would be the prerequisite to achieve a fluent crystallization. The more unstable state of Ti atoms in the TiO₂ layer in the [TOTOSHSH] sequence may have induced a more chance to form a better crystallized STO film.

The enhanced perovskite lattice formation is also confirmed by the analysis of the crystal structure and electrical property. The crystal structures of STO films deposited by [TOTOSHSH] and [TOSO] were investigated using XRD and TEM analysis (Figure 6). STO films were in situ crystallized

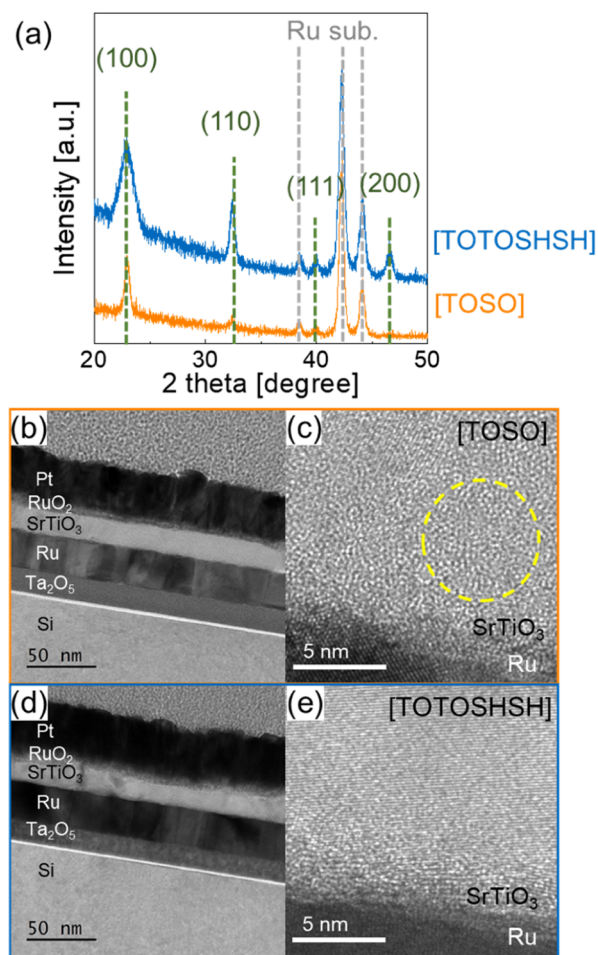


Figure 6. (a) XRD spectra of the STO films deposited by [TOTOSHSH] (H₂O) and [TOSO] (O₃) sequences. (b–e) Cross-sectional image of the MIM structure for electrical measurements. The STO films in the MIM structure was deposited by (b,c) [TOSO] and (d,e) [TOTOSHSH] sequence, respectively. (c,e) Magnified image of the STO film right above the bottom Ru electrode from (c) image of (b) and (e) image of (d).

with the aid of 4 nm thick seed layers that were deposited by [TOTOSHSH] and [TOSO], respectively, and crystallized at 650 °C in an N₂ atmosphere by a rapid thermal annealing system.¹² In the XRD spectra of Figure 6a, the peaks correspond to (100), (110), and (200) and exhibited different relative intensities; the film grown by the [TOTOSHSH]

sequence exhibited a stronger peak intensity than that by the [TOSO] sequence, whereas the peaks from the Ru bottom electrode layer showed similar intensities, indicating that the crystal structure of the STO film by the [TOTOSHSH] sequence had a higher crystalline quality than that by the TOSO sequence. The crystal structure difference was also clearly observed in the TEM images. Figure 6b,c shows the low-magnification and high-resolution TEM images, respectively, of the STO film by the [TOSO] sequence, which revealed that a significant portion of the film was not crystallized, as indicated by the yellow circle in Figure 6c. However, the images of the STO film by the [TOTOSHSH] sequence, shown in Figure 6d,e, revealed a much better crystallized structure with a rare involvement of amorphous regions. These findings corroborated the Sr XPS and XRD data. The electrical property of the MIM capacitor employing an STO film as an insulator layer that adopted the crystallized STO seed layer for in situ crystallization also revealed the higher crystallinity of the STO film by the [TOTOSHSH] sequence compared with the film by the [TOSO] sequence. Because the bulk dielectric constant (k) is a representative indicator of the crystalline quality of the STO film, it was estimated from the inverse slope of physical thickness (t_{phy})—equivalent oxide thickness (t_{ox}) plot, where $t_{\text{ox}} = t_{\text{phy}}(3.9/k)$.^{15,16,25} The k value of the STO film by the [TOSO] sequence was measured to be 98, whereas the k value by [TOTOSHSH] was as high as 236 (Figure 7a), which is the

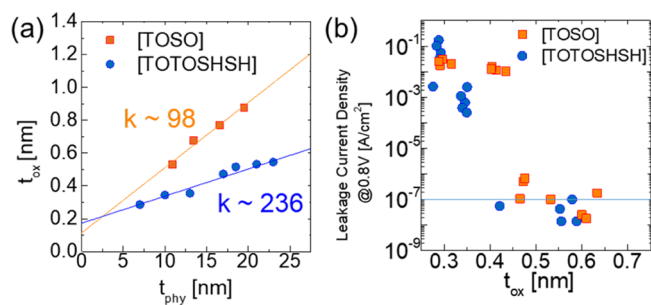


Figure 7. (a) Variation of equivalent oxide thickness as a function of the physical thickness of STO films and (b) the J – t_{ox} plot for the MIM structure with the STO films deposited by [TOSO] and [TOTOSHSH] sequences.

highest value reported from ALD STO films. The bulk dielectric constant of the [TOSO] film was somewhat lower than the reported value²⁶ because the substrate, TE, and annealing condition were slightly changed. However, in this study, other conditions except for the process sequence, [TOSO] and [TOTOSHSH], were carefully controlled. Therefore, these data can be regarded as a strong support for the better crystallinity of the STO film by the [TOTOSHSH] sequence compared with the film by the [TOSO] sequence. Figure 7b shows the summary of the electrical performances of the two types of films, which shows the variation of J estimated at +0.8 V as a function of t_{ox} . As reported previously for STO and many other DRAM capacitor dielectric films, the leakage current density (J) increases rapidly with decreasing t_{ox} value.^{1,4} For stable DRAM applications, J of an MIM capacitor must be $<10^{-7}$ A/cm². The two types of films showed similar critical t_{ox} values (0.42–0.45 nm) that are seemingly inconsistent with the higher k value of the film by the [TOTOSHSH] sequence. However, as can be understood from the higher portion of the TiO_{2-x} phase in this film shown in Figure 4, the film had a

higher defect density making them slightly leakier. Therefore, the overall electrical performance was not improved as much as the k value was. Although the bulk dielectric constants of STO films obtained in this study are quite reliable, the Y-axis intercepts in t_{ox} versus t_{phy} graph had relatively low reliability. Because the interfacial properties between the STO film and the TE or the bottom electrode have a main role in determining the Y-intercept of Figure 7a, which is vulnerable to the subtle change in the deposition and substrate conditions, the main argument about the bulk property of STO films in this study would not be significantly influenced. Despite the very high k value of the [TOTOSHS] film, the involvement of the relatively high value of interfacial t_{ox} (~ 0.18 nm) prohibited the ultimate scaling of t_{ox} down to < 0.4 nm. Further efforts to reduce the deleterious interface property and to improve the overall electric performance are ongoing.

4. CONCLUSION

The incorporation behaviors of Ti and Sr atoms into the STO films during the ALD process were quantitatively examined depending on the detailed process conditions, especially the types of oxygen sources, H_2O or O_3 , injected before and after the metal precursor injection steps. For the case of Ti incorporation, O_3 injection prior to the Ti precursor injection results in an almost two times higher incorporation rate compared to the case with H_2O injection at the same process step. The Sr incorporation behavior showed a similar trend. The O_3 -pulsed surface before the Sr precursor injection resulted in an almost doubled incorporation rate compared with the H_2O -pulsed surface. These behaviors indicate that the first half ALD cycle during one ALD subcycle dominates the overall ALD behavior, and the O_3 -terminated surface has an almost doubled reactivity toward the Ti and Sr precursors. The detailed and quantitative estimation of the incorporation rate of Sr atoms revealed that some of the oxygen atoms in the previously deposited TiO_2 layer are taken up by the reaction with incoming Sr precursors, which results in the TiO_{2-x} components in the STO film. The O_3 pulse step after the Sr precursor injection step dominantly reoxidized the reduced TiO_{2-x} components, whereas its influence on the Sr incorporation was minimal. However, such an effect was not obvious when H_2O was pulsed after the Sr precursor injection step, resulting in the higher portion of remaining TiO_{2-x} in the final STO film. Nonetheless, this was not detrimental to the crystallization of the STO film into the desired perovskite structure. Rather, the crystallization was more enhanced compared with the film grown by the other sequence utilizing the O_3 pulse after the Sr precursor injection. This is corroborated by the structural and electrical analysis of the STO film. It was considered that the more defective nature of the TiO_2 layer for the [TOTOSHS] process sequence resulted in a better quality perovskite-structured STO film. As a consequence, the highest bulk dielectric constant of 236 was achieved, but the remaining defects within the film deteriorated the leakage properties. Therefore, the overall electrical performances represented by the J versus t_{ox} property were similar with the films grown by [TOSO]. The method adopted in this work can be easily extended to other multicomponent ALD study, which can provide insightful viewpoints for the specific ALD process.

■ ASSOCIATED CONTENT

Supporting Information

The Supporting Information is available free of charge on the ACS Publications website at DOI: 10.1021/acsami.7b18807.

ALD saturation behavior of SrO film using H_2O as the oxygen source (PDF)

■ AUTHOR INFORMATION

Corresponding Authors

*E-mail: woongkyul.ee@northwestern.edu (W.L.).

*E-mail: cheolsh@snu.ac.kr (C.S.H.).

ORCID

Cheol Seong Hwang: 0000-0002-6254-9758

Author Contributions

^{||}M.J.C. and W.J. equally contributed to this work.

Notes

The authors declare no competing financial interest.

■ ACKNOWLEDGMENTS

This work was supported by the Future Semiconductor Device Technology Development Program (10047231) through MOTIE (Ministry of Trade, Industry, & Energy) and KSRC (Korea Semiconductor Research Consortium) [Project Name: Development of mass production technology for DRAM capacitor].

■ REFERENCES

- (1) Hwang, C. S. *Atomic Layer Deposition for Semiconductors*; Springer: New York, 2014.
- (2) Leskelä, M.; Ritala, M. Atomic Layer Deposition Chemistry: Recent Developments and Future Challenges. *Angew. Chem., Int. Ed. Engl.* **2003**, *42*, 5548–5554.
- (3) Knez, M.; Nielsch, K.; Niinistö, L. Synthesis and Surface Engineering of Complex Nanostructures by Atomic Layer Deposition. *Adv. Mater.* **2007**, *19*, 3425–3438.
- (4) Hwang, C. S. Atomic Layer Deposition for Microelectronic Applications. *Atomic Layer Deposition of Nanostructured Materials*; Wiley-VCH: Weinheim, Germany, 2011; pp 159–192.
- (5) Marichy, C.; Bechelany, M.; Pinna, N. Atomic Layer Deposition of Nanostructured Materials for Energy and Environmental Applications. *Adv. Mater.* **2012**, *24*, 1017–1032.
- (6) Heyman, A.; Musgrave, C. B. A Quantum Chemical Study of the Atomic Layer Deposition of Al_2O_3 Using AlCl_3 and H_2O as Precursors. *J. Phys. Chem. B* **2004**, *108*, 5718–5725.
- (7) Kopalko, K.; Godlewski, M.; Domagala, J. Z.; Lusakowska, E.; Minikayev, R.; Paszkowicz, W.; Szczerbakow, A. Monocrystalline ZnO Films on GaN/ Al_2O_3 by Atomic Layer Epitaxy in Gas Flow. *Chem. Mater.* **2004**, *16*, 1447–1450.
- (8) Guzewicz, E.; Godlewski, M.; Wachnicki, L.; Krajewski, T. A.; Luka, G.; Gieraltowska, S.; Jakiela, R.; Stonert, A.; Lisowski, W.; Krawczyk, M.; Sobczak, J. W.; Jablonski, A. ALD Grown Zinc Oxide with Controllable Electrical Properties. *Semicond. Sci. Technol.* **2012**, *27*, 074011.
- (9) Matero, R.; Rahtu, A.; Ritala, M. In Situ Quadrupole Mass Spectrometry and Quartz Crystal Microbalance Studies on the Atomic Layer Deposition of Titanium Dioxide from Titanium Tetrachloride and Water. *Chem. Mater.* **2001**, *13*, 4506–4511.
- (10) Gu, W.; Tripp, C. P. Role of Water in the Atomic Layer Deposition of TiO_2 on SiO_2 . *Langmuir* **2005**, *21*, 211–216.
- (11) Lee, S. W.; Han, J. H.; Kwon, O. S.; Hwang, C. S. Influences of a Crystalline Seed Layer during Atomic Layer Deposition of SrTiO_3 Thin Films Using $\text{Ti}(\text{O}-i\text{Pr})_2(\text{thd})_2$, $\text{Sr}(\text{thd})_2$, and H_2O . *J. Electrochem. Soc.* **2008**, *155*, G253–G257.

- (12) Lee, W.; Jeon, W.; An, C. H.; Chung, M. J.; Kim, H. J.; Eom, T.; George, S. M.; Park, B. K.; Han, J. H.; Kim, C. G.; Chung, T.-M.; Lee, S. W.; Hwang, C. S. Improved Initial Growth Behavior of SrO and SrTiO₃ Films Grown by Atomic Layer Deposition Using {Sr-(demamp)(tmhd)}₂ as Sr-Precursor. *Chem. Mater.* **2015**, *27*, 3881–3891.
- (13) Kosola, A.; Putkonen, M.; Johansson, L.-S.; Niinistö, L. Effect of Annealing in Processing of Strontium Titanate Thin Films by ALD. *Appl. Surf. Sci.* **2003**, *211*, 102–112.
- (14) Vehkamäki, M.; Hänninen, T.; Ritala, M.; Leskelä, M.; Sajavaara, T.; Rauhala, E.; Keinonen, J. Atomic Layer Deposition of SrTiO₃ Thin Films from a Novel Strontium Precursor-Strontium-Bis(tri-Isopropyl Cyclopentadienyl). *Chem. Vap. Deposition* **2001**, *7*, 75–80.
- (15) Lee, W.; Han, J. H.; Jeon, W.; Yoo, Y. W.; Lee, S. W.; Kim, S. K.; Ko, C.-H.; Lansalot-Matras, C.; Hwang, C. S. Atomic Layer Deposition of SrTiO₃ Films with Cyclopentadienyl-Based Precursors for Metal–Insulator–Metal Capacitors. *Chem. Mater.* **2013**, *25*, 953–961.
- (16) Lee, S. W.; Han, J. H.; Han, S.; Lee, W.; Jang, J. H.; Seo, M.; Kim, S. K.; Dussarrat, C.; Gatineau, J.; Min, Y.-S.; Hwang, C. S. Atomic Layer Deposition of SrTiO₃ Thin Films with Highly Enhanced Growth Rate for Ultrahigh Density Capacitors. *Chem. Mater.* **2011**, *23*, 2227–2236.
- (17) Kil, D.-S.; Lee, J.-M.; Roh, J.-S. Low-Temperature ALD Growth of SrTiO₃ Thin Films from Sr β-Diketonates and Ti Alkoxide Precursors Using Oxygen Remote Plasma as an Oxidation Source. *Chem. Vap. Deposition* **2002**, *8*, 195–197.
- (18) Kwon, O. S.; Kim, S. K.; Cho, M.; Hwang, C. S.; Jeong, J. Chemically Conformal ALD of SrTiO₃ Thin Films Using Conventional Metallorganic Precursors. *J. Electrochem. Soc.* **2005**, *152*, C229–C236.
- (19) Popovici, M.; Tomida, K.; Swerts, J.; Favia, P.; Delabie, A.; Bender, H.; Adelman, C.; Tielens, H.; Brijs, B.; Kaczer, B.; Pawlak, M. A.; Kim, M.-S.; Altimime, L.; Van Elshocht, S.; Kittl, J. A. A Comparative Study of the Microstructure-Dielectric Properties of Crystalline SrTiO₃ ALD Films Obtained via Seed Layer Approach. *Phys. Status Solidi* **2011**, *208*, 1920–1924.
- (20) Lee, S. W.; Han, J. H.; Kim, S. K.; Han, S.; Lee, W.; Hwang, C. S. Role of Interfacial Reaction in Atomic Layer Deposition of TiO₂ Thin Films Using Ti(O-iPr)₂(tmhd)₂ on Ru or RuO₂ Substrates. *Chem. Mater.* **2011**, *23*, 976–983.
- (21) Young, M. J.; Hare, C. D.; Cavanagh, A. S.; Musgrave, C. B.; George, S. M. Rapid Growth of Crystalline Mn₅O₈ by Self-Limited Multilayer Deposition Using Mn(ETCp)₂ and O₃. *ACS Appl. Mater. Interfaces* **2016**, *8*, 18560–18569.
- (22) Eom, T.; Gwon, T.; Yoo, S.; Choi, B. J.; Kim, M.-S.; Buchanan, I.; Ivanov, S.; Xiao, M.; Hwang, C. S. Combined Ligand Exchange and Substitution Reactions in Atomic Layer Deposition of Conformal Ge₂Sb₂Te₃ Film for Phase Change Memory Application. *Chem. Mater.* **2015**, *27*, 3707–3713.
- (23) Gwon, T.; Eom, T.; Yoo, S.; Yoo, C.; Park, E.-s.; Kim, S.; Kim, M.-S.; Buchanan, I.; Xiao, M.; Ivanov, S.; Hwang, C. S. Atomic Layer Deposition of GeTe and Ge–Sb–Te Films Using HGeCl₃, Sb(OC₂H₅)₃, and {(CH₃)₃Si}₂ Te and Their Reaction Mechanisms. *Chem. Mater.* **2017**, *29*, 8065–8072.
- (24) Jeon, W.; Lee, W.; Yoo, Y. W.; An, C. H.; Han, J. H.; Kim, S. K.; Hwang, C. S. Chemistry of Active Oxygen in RuO_x and Its Influence on the Atomic Layer Deposition of TiO₂ Films. *J. Mater. Chem. C* **2014**, *2*, 9993–10001.
- (25) Lee, S. W.; Kwon, O. S.; Han, J. H.; Hwang, C. S. Enhanced Electrical Properties of SrTiO₃ Thin Films Grown by Atomic Layer Deposition at High Temperature for Dynamic Random Access Memory Applications. *Appl. Phys. Lett.* **2008**, *92*, 222903.
- (26) Lee, W.; Han, J. H.; Lee, S. W.; Han, S.; Jeon, W. J.; Hwang, C. S. Controlling the Initial Growth Behavior of SrTiO₃ Films by Interposing Al₂O₃ Layers between the Film and the Ru Substrate. *J. Mater. Chem.* **2012**, *22*, 15037–15044.
- (27) Holme, T. P.; Prinz, F. B. Atomic Layer Deposition and Chemical Vapor Deposition Precursor Selection Method Application to Strontium and Barium Precursors. *J. Phys. Chem. A* **2007**, *111*, 8147–8151.
- (28) Tomczak, Y.; Knapas, K.; Haukka, S.; Kemell, M.; Heikkilä, M.; Ceccato, M.; Leskelä, M.; Ritala, M. In Situ Reaction Mechanism Studies on Atomic Layer Deposition of Al_xSi_yO_z from Trimethylaluminum, Hexakis(ethylamino)disilane, and Water. *Chem. Mater.* **2012**, *24*, 3859–3867.
- (29) Lee, Y.; Sun, H.; Young, M. J.; George, S. M. Atomic Layer Deposition of Metal Fluorides Using HF-Pyridine as the Fluorine Precursor. *Chem. Mater.* **2016**, *28*, 2022–2032.
- (30) Lu, J.; Low, K.-B.; Lei, Y.; Libera, J. A.; Nicholls, A.; Stair, P. C.; Elam, J. W. Toward Atomically-Precise Synthesis of Supported Bimetallic Nanoparticles Using Atomic Layer Deposition. *Nat. Commun.* **2014**, *5*, 3264.
- (31) Juppo, M.; Rahtu, A.; Ritala, M.; Leskelä, M. In Situ Mass Spectrometry Study on Surface Reactions in Atomic Layer Deposition of Al₂O₃ Thin Films from Trimethylaluminum and Water. *Langmuir* **2000**, *16*, 4034–4039.
- (32) Rahtu, A.; Kukli, K.; Ritala, M. In Situ Mass Spectrometry Study on Atomic Layer Deposition from Metal (Ti, Ta, and Nb) Ethoxides and Water. *Chem. Mater.* **2001**, *13*, 817–823.
- (33) Goldstein, D. N.; McCormick, J. A.; George, S. M. Al₂O₃ Atomic Layer Deposition with Trimethylaluminum and Ozone Studied by in Situ Transmission FTIR Spectroscopy and Quadrupole Mass Spectrometry. *J. Phys. Chem. C* **2008**, *112*, 19530–19539.
- (34) Yanguas-Gil, A.; Libera, J. A.; Elam, J. W. In Situ FTIR Characterization of Growth Inhibition in Atomic Layer Deposition Using Reversible Surface Functionalization. *ECS Trans.* **2013**, *50*, 43–51.
- (35) Qin, X.; Wallace, R. M. In Situ Plasma-Enhanced Atomic Layer Deposition Half Cycle Study of Al₂O₃ on AlGaN/GaN High Electron Mobility Transistors. *Appl. Phys. Lett.* **2015**, *107*, 081608.
- (36) Methaapanon, R.; Bent, S. F. Comparative Study of Titanium Dioxide Atomic Layer Deposition on Silicon Dioxide and Hydrogen-Terminated Silicon. *J. Phys. Chem. C* **2010**, *114*, 10498–10504.
- (37) Lee, S. W.; Choi, B. J.; Eom, T.; Han, J. H.; Kim, S. K.; Song, S. J.; Lee, W.; Hwang, C. S. Influences of Metal, Non-Metal Precursors, and Substrates on Atomic Layer Deposition Processes for the Growth of Selected Functional Electronic Materials. *Coord. Chem. Rev.* **2013**, *257*, 3154–3176.
- (38) Vehkamäki, M. Growth of SrTiO₃ and BaTiO₃ Thin Films by Atomic Layer Deposition. *Electrochem. Solid-State Lett.* **1999**, *2*, 504–506.
- (39) Chen, X.; Liu, L.; Liu, Z.; Marcus, M. A.; Wang, W.-C.; Oyler, N. A.; Grass, M. E.; Mao, B.; Glans, P.-A.; Yu, P. Y.; Guo, J.; Mao, S. S. Properties of Disorder-Engineered Black Titanium Dioxide Nanoparticles through Hydrogenation. *Sci. Rep.* **2013**, *3*, 1510.
- (40) Li, Y.; Wang, Q.; An, M.; Li, K.; Wehbe, N.; Zhang, Q.; Dong, S.; Wu, T. Nanoscale Chemical and Valence Evolution at the Metal/Oxide Interface: A Case Study of Ti/SrTiO₃. *Adv. Mater. Interfaces* **2016**, *3*, 1600201.
- (41) Baeumer, C.; Schmitz, C.; Ramadan, A. H. H.; Du, H.; Skaja, K.; Feyer, V.; Müller, P.; Arndt, B.; Jia, C.-L.; Mayer, J.; De Souza, R. A.; Schneider, C. M.; Waser, R.; Dittmann, R. Spectromicroscopic Insights for Rational Design of Redox-Based Memristive Devices. *Nat. Commun.* **2015**, *6*, 8610.
- (42) Lenser, C.; Koehl, A.; Slipukhina, I.; Du, H.; Patt, M.; Feyer, V.; Schneider, C. M.; Lezaic, M.; Waser, R.; Dittmann, R. Formation and Movement of Cationic Defects During Forming and Resistive Switching in SrTiO₃ Thin Film Devices. *Adv. Funct. Mater.* **2015**, *25*, 6360–6368.
- (43) Szot, K.; Speier, W.; Breuer, U.; Meyer, R.; Szade, J.; Waser, R. Formation of Micro-Crystals on the (100) Surface of SrTiO₃ at Elevated Temperatures. *Surf. Sci.* **2000**, *460*, 112–128.